Solvent Effects on Peroxynitrite Structure and Properties from QM/MM Simulations

Mariano C. González Lebrero, Laura L. Perissinotti, and Darío A. Estrin*

Departamento de Química Inorgánica, Analítica y Química Física - INQUIMAE-CONICET, Facultad de Ciencias Exactas y Naturales, Universidad de Buenos Aires, Ciudad Universitaria, Pabellón 2, C1428EHA, Buenos Aires, Argentina

Received: July 29, 2005; In Final Form: August 30, 2005

We have investigated the structure and the vibrational spectrum of peroxynitrite anion in aqueous solution by means of combined quantum-classical (QM/MM) molecular dynamics simulations. In our QM/MM scheme, the reactant was modeled using density functional theory with a Gaussian basis set and the solvent was described using the mean-field TIP4P and the polarizable TIP4P-FQ force fields. The choice of basis sets, functionals and force field parameters has been validated by performing calculations on isolated peroxynitrite and on small peroxynitrite−water complexes. Poor values for isolated peroxynitrite structural properties and vibrational frequencies are found for most ab initio methods, particularly regarding the ON−OO$^-$ bond distance and the harmonic stretching frequency, probably due to the singlet−triplet instability found in the HF wave function. On the other hand, DFT methods yield results in better agreement with high level CCSD(T) ab initio calculations. We have computed the vibrational spectrum for aqueous peroxynitrite by calculating the Fourier transform of the velocity autocorrelation function extracted from the QM-MM molecular dynamics simulations. Our computational scheme, which allows for the inclusion of both anharmonicity and solvent effects, is able to clarify previous discrepancies regarding the experimental spectra assignments and to shed light on the subtle interplay between solvation and peroxynitrite structure and properties.

1. Introduction

Peroxynitrite anion (ONOO$^-$), is a stable species formed by the reaction of superoxide with nitric oxide in biological environments.[1] Peroxynitrite is very stable in alkaline solutions,[2] whereas peroxynitrous acid, formed in the body by protonation of ONOO$^-$, isomerizes at neutral pH to nitric acid with a rate constant of 0.65 s^{-1} at 37 °C.[3] This species exhibits a strong cellular toxicity in humans due to its action as oxidant of sulfhydryl groups, phospholipids, and DNA. It has also been reported that peroxynitrite may be involved in the nitration and hydroxylation of aromatic groups and is capable to inhibit several key enzymes.[4] Due to its role in physiological and physical chemistry, peroxynitrite and its conjugate acid have been the subject of many experimental[5−8] and theoretical investigations.[9−19]

Due to the π character of the NO3 bond, peroxynitrite is expected to exist in two conformations, the cis and trans isomers. (Figure 1) An X-ray structure analysis of tetramethylammonium peroxynitrite indicates that peroxynitrite crystallizes in the cis conformation.[5] The Raman spectrum in aqueous solution has also been assigned to the cis isomer.[16] The infrared spectra of both cis and trans alkali-metal peroxoxynitrites have been measured at low temperature in solid Ar.[8]

Early Hartree−Fock calculations predicted that the trans form is the global minimum.[9] On the other hand, and in agreement with the experimental evidence, correlated methods predict that the cis conformer is more stable than the trans isomer.[17] Tsai et al. investigated the conformational preference of peroxynitrite by using high level correlated coupled cluster techniques, as well as DFT methods.[17] They predicted a preference for the cis form over the trans by 2−4 kcal/mol and a torsional cis−trans interconversion barrier of 21−27 kcal/mol.[17] The thermochemistry of isolated peroxynitrite decomposition has been investigated using a variety of ab initio and DFT schemes by Mak et al. These authors found significant flaws in the peroxynitrite geometry prediction at the QCISD level.[18] Atomization energies of isolated peroxynitrite have been computed at the quantum Monte Carlo, B3LYP and MP2 levels of theory by Harkless et al., finding significant errors in the B3LYP and MP2 predictions.[19] Tsai et al. also considered solvent effects by means of continuum model calculations.[17] Solvent effects have also been modeled by including a small number of water molecules in the calculations.[20] The complexes with the water molecules coordinated to the formally negative O4 oxygen atom turned out to be more stable.[20] An explicit solvent classical Monte Carlo simulation of aqueous peroxynitrite, using atomic charges dependent on the torsion angle, has yielded a free energy torsional barrier of 18−24 kcal/mol.[10] The conformational equilibria of the conjugate peroxynitrous acid in a vacuum and in aqueous solution has also been studied at the DFT level by means of Car−Parrinello molecular dynamics, obtaining rotational barriers of 55 and 89 ± 10 kJ/mol, respectively.[11]

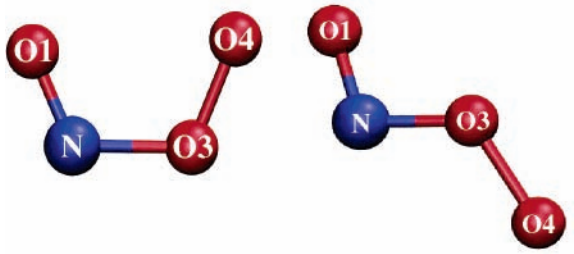

Figure 1. Schematic representation of peroxynitrite cis (left) and trans (right) isomers

* Corresponding author. E-mail: dario@qi.fcen.uba.ar. Phone: 54-11-4576-3368. Fax: 54-11-4576-3341.

10.1021/jp054224l CCC: $30.25
Published on Web 10/01/2005

The experimental Raman spectrum of peroxynitrite in aqueous solution has been assigned on the basis of electronic structure calculations by Tsai et al.[16,17] In those works, a very intense and broad band in the Raman spectrum centered at 642 cm^{-1}, assigned to the ONOO torsion, was predicted to be too low by 100−150 cm^{-1}. Solvent effects (based on continuum models or by computations including a small number of explicit solvent molecules) and anharmonicity were found to be unlikely sources of this disagreement.[17] An alternative interpretation of the experimental spectrum, based on the assumption that the cis and trans conformations have comparable stabilities and are in rapid equilibrium at room temperature, has also been proposed.[21]

In this work, we shed light on the structural and vibrational properties of peroxynitrite in aqueous solution by applying a combined quantum-classical (QM/MM) computational methodology that incorporates in a natural way anharmonic and explicit solvation effects. The basic approximation of QM/MM methods involves partitioning the system under investigation into one subsystem that requires a rigorous quantum treatment and an environment that is normally treated using empirical force fields. In addition to the lower computational cost compared to a full QM calculation, these methods have the advantage that they are based on concepts closely related to common chemical argumentation.[22,23] QM/MM schemes have been employed successfully to investigate vibrational properties of solvated species.[24−26]

The article is organized as follows: section 2 contains an outline of our model and simulation methods. Section 3 contains the results of peroxynitrite structure, vibrational frequencies and Raman intensities computed at several ab initio and DFT levels of theory and peroxynitrite−water complexes calculations at the QM and QM/MM levels. In section 4 we present the results obtained from the QM/MM molecular dynamics simulations. Finally, concluding remarks are presented in section 5.

2. Model and Simulation Methods

Hybrid QM/MM Hamiltonian. Our computational scheme was constructed by partitioning the system into a quantum-mechanical (QM) and a classical-mechanical (MM) subsystems. Considering a configuration of N_c atoms in the MM subsystem with coordinates and partial charges $\{R_l, q_l, l = 1, ..., N_c\}$ and N_q atoms in the QM sub-system with coordinates and nuclear charges $\{\tau_a, z_a, a = 1, ..., N_q\}$, we propose the following expression for the ground state, Born−Oppenheimer potential energy surface that drives the dynamics of the nuclei:

$$E[\{R_i\},\{\tau_\alpha\}] = E_{KS} + E_{QM-MM} + E_{MM} \quad (1)$$

where the first term is a purely QM piece given by the standard Kohn−Sham expression.[27] The second term in eq 1 accounts for the coupling of the QM and MM subsystems and is given by

$$E_{QM-MM} = \sum_{l=1}^{N_C} q_l \int \frac{\rho(r)}{|r - R_l|}\,dr + \sum_{l=1}^{N_C}\sum_{\alpha=1}^{N_q}\left[v_{LJ}(|R_l - \tau_\alpha|) + \frac{q_l z_\alpha}{|R_l - \tau_\alpha|}\right] \quad (2)$$

where v_{LJ} is the Lennard-Jones potential between the classical and quantum part of the system and $\rho(r)$ is the electron density of the QM subsystem. The last term in eq 1 represents the potential energy contribution from the classical solvent potential, treated with the TIP4P mean-field[28] or the polarizable fluctuating charge TIP4P-FQ schemes.[29] In the latter, polarization effects are explicitly incorporated by allowing the partial charges to fluctuate along the simulation run. The simultaneous time evolution of spatial coordinates and partial charges is obtained by employing an extended Lagrangian approach. More details about our fluctuating charge implementation of the QM-MM scheme have been previously reported.[30]

For the QM region, computations were performed at the local density approximation (LDA) and generalized gradient approximation (GGA) level, using the BP86[31−33] and PBE combination of exchange and correlation functionals.[34] Gaussian basis sets of double-ζ plus polarization quality were employed for the expansion of the one-electron orbitals.[35] The electronic density was also expanded in an auxiliary basis set;[35] the coefficients for the fit were computed by minimizing the error in the Coulomb repulsion energy. The use of this procedure results in an important speedup of the computations. The electronic density was computed every MD step.

Molecular Dynamics Simulations. In all our simulation experiments, the coordinate Verlet algorithm[36] was employed to integrate Newton's equations of motion with a time step of 0.2 and 0.1 fs for TIP4P and TIP4P-FQ simulations, respectively. All fictitious masses associated with the charge dynamics were set to 6.0×10^{-5} kcal/mol $(ps/e)^2$. In addition, a Berendsen thermostat set at 2 K was coupled to the partial charges in the TIP4P-FQ simulation to maintain the charge degrees of freedom decoupled from the nuclear motion.[37] Constraints associated with the intramolecular distances in water were treated using the SHAKE algorithm.[38] The Lennard-Jones parameters for the quantum subsystem atoms are ϵ and σ of 0.200 and 0.155 kcal/mol, and 3.900 and 3.154 Å, for N and O, respectively. The solute was solvated in a cubic box of size $a = 24$ Å, containing 497 water molecules. Periodic boundary conditions with a group cutoff were used for solvent−solvent interactions. A cutoff scheme was also employed for dealing with solute−solvent interactions (See Appendix for more details.) Initial configurations were generated from preliminary 100 ps classical equilibration runs in which the quantum solute was replaced by a rigid peroxynitrite with partial charges obtained from a Mulliken population analysis. At $t = 0$, the classical solute is replaced by a peroxynitrite described at the DFT level, according to the hybrid methodology described above. An additional 1 ps of equilibration was performed using the QM-MM scheme. During the simulations, the temperature was held constant at 298 K by the Berendsen thermostat.[37] The solute and the rest of the system were coupled separately to the temperature bath. In all cases, 20 ps of dynamics were used for production runs.

To obtain the vibrational frequencies corresponding to each normal mode, we transformed the dynamical trajectory into the normal modes coordinates of the isolated solute. The time derivatives of these new set of coordinates, which correspond to the velocity in this coordinate system, were computed. Finally, the vibrational density of states (DOS) was obtained from the Fourier transform of the velocity time correlation function. The use of this procedure, instead of employing the velocity autocorrelation function in the original coordinate system, results in a significant numerical improvement, and facilitates assignments. This approach results in the evaluation of the actual vibrational bands without resorting to harmonic approximations.

Electronic Structure Calculations for Isolated Peroxynitrite. The ab initio calculations for the isolated system were performed using the Gaussian 98 code,[39] with the same basis set used in the QM/MM scheme. Ab initio geometry optimizations and normal modes calculations have been performed at

TABLE 1: Predicted Harmonic Vibrational Frequencies (cm^{-1}) for Isolated Peroxynitrite at Different Levels of Theory[a]

	NO1 str	O1NO3 bend	O3O4 str	NO3 str	O4O3NO1 tors	NO3O4 bend
HF(ms)	1775	1006	766	1336	451	386
HF(ls)	1767	1028	816	1310	470	398
MP2(ms)	1409 (15)	936 (14)	839 (51)	1007 (100)	549 (0)	346 (35)
MP2(ls)	1436	964	867	988	569	360
CCSD	1535	900	793	1002	485	348
CCSD(T)	1460	924	814	715	488	326
LDA	1484	1011	850	667	508	306
BP86	1468	1016	832	503	478	291
PBE(ms)	1476	1026	841	522	485	297
PBE(ls)	1476	1017	845	539	495	307
B3LYP	1508 (74)	979 (23)	841 (69)	775 (100)	499 (0)	330 (35)

[a] HF, MP2, and PBE calculations have been performed for a medium size DZVP (ms) and a larger size 6-31+G(3df,2p) basis sets (ls). Relative Raman intensities are given in parentheses for MP2 and B3LYP calculations.

the Hartree−Fock, MP2, CCSD coupled cluster single and double excitations, CCSD(T) coupled cluster single and double excitations including triple excitations noniteratively. DFT calculations have been performed at the local density approximation (LDA),[31] generalized gradient approximation (BP86[32,33] and PBE[34]), and at the hybrid B3LYP[40] levels. To explore the sensitivity of the results with the quality of the basis sets, we have also performed HF, MP2, and DFT(PBE) calculations with the 6-31+g(3df,2p) basis set. Raman intensities were also computed in selected cases.

3. Isolated Peroxynitrite

We present in Table 1 the harmonic vibrational frequencies obtained for the ab initio and DFT calculations of isolated peroxynitrite. It can be seen from the table that there is a very strong sensitivity of the N−O3 stretching frequency with the level of theory. This stretching frequency ranges from 503 cm^{-1} at the BP86 level to 1303 cm^{-1} at the HF level. It is also interesting to note the large difference between the computed N−O3 frequency at the CCSD (1002 cm^{-1}) and CCSD(T) levels (715 cm^{-1}). One possible explanation for this fact may lie on the singlet−triplet Hartree−Fock wave function instability found for peroxynitrite. A similar singlet−triplet instability has been found for alkali peroxynitrites by Tsai et al.[20] and has been related to the poor performance of HF based methods in describing these systems. On the other hand, both the more sophisticated CCSD(T) and the various DFT schemes seem to be able to deal with this class of systems, yielding relatively similar results.

The assignment of the experimental Raman spectra in aqueous solution performed by Tsai et al.[16,17] proposed, on the basis of MP2 and CCSD calculations and of isotope shifts, that the experimental broad and intense band at 642 cm^{-1} corresponded to the ONOO torsion. These authors suggested that the computationally predicted N−O stretching frequency at about 1000 cm^{-1} is not seen because it coincides with a peak in the nitrate spectrum. However, this is not consistent with the fact that the torsional mode exhibits an extremely low Raman computed intensity (Table 1). A more convincing explanation of the experimental spectrum is that the broad and intense 642 cm^{-1} band corresponds to the O3−N stretching, whereas the torsion mode is practically Raman inactive. This explains the computed results for isolated peroxynitrite and, as will be shown later in the paper, is consistent with the QM/MM results in solution.

Selected optimized structural parameters for isolated peroxynitrite are presented in Table 2. The results show a significant dispersion of the predicted NO3 bond distances with the level of theory used, consistently with the trends in the harmonic frequencies presented in Table 1. The low resolution X-ray

TABLE 2: Selected Optimized Geometrical Parameters for Isolated Peroxynitrite Obtained at Different Levels of Theory[a]

	NO1	NO3	O1NO3	O3O4	O4O3N
HF(ms)	1.190	1.270	118.6	1.431	118.4
HF(ls)	1.179	1.267	118.7	1.403	118.3
MP2(ms)	1.258	1.355	115.1	1.383	117.8
MP2(ls)	1.233	1.339	115.2	1.352	117.6
CCSD	1.232	1.344	116.5	1.427	117.3
CCSD(T)	1.244	1.379	115.6	1.417	117.3
LDA	1.231	1.410	113.7	1.346	117.0
BP86	1.242	1.467	114.0	1.376	117.4
PBE(ms)	1.240	1.458	114.1	1.371	117.5
PBE(ls)	1.226	1.438	114.6	1.360	117.5
B3LYP	1.232	1.367	116.0	1.395	118.5
X-ray	1.16	1.35	118.3	1.41	111.3

[a] HF, MP2, and PBE calculations have been performed for a medium size (ms) and a larger size basis sets (ls).

results obtained by Wörle et al. for tetramethylammonium peroxynitrite are also included in Table 2. [5] It is clear from the inspection of NO3 bond distances that the degree of π bonding is very dependent on the employed electronic structure scheme. This has been recently noted by Mak et al., who found strikingly different peroxynitrite molecular geometries for QCISD and CCSD computations.[18] HF predicts a shorter and consistently stronger bond than correlated ab initio methods. DFT schemes yield longer bond distances than CCSD(T), consistently with the larger stretching frequency predicted at that level.

Structure and Energetics of Peroxynitrite−Water Complexes. To assess the quality of our approach, we performed a series of preliminary runs to compute the energetics and geometrical parameters of minimum energy configurations of some relevant quantum-classical model dimers and trimers. In all cases, we performed QM/MM computations in which peroxynitrite was treated quantum-mechanically at the DFT PBE level and the water molecules classically. For the sake of comparison, full quantum-mechanical calculation at the DFT level were also performed at the PBE level. Cointerpoise estimations were considered for correcting the basis set superposition errors in binding energies.

Consistently with previous results, we have found that the most favorable site for peroxynitrite solvation is O4. We have found that the computed QM/MM binding energies agree reasonably well with those computed at the DFT level. The structures of the corresponding QM-MM optimized dimer and trimer are presented in Figure 2. The binding energies are presented in Table 3. The overall agreement between the full QM and the hybrid QM-MM calculations is reasonable. Our results for binding energies and structural parameters are also consistent with B3LYP calculations reported by Musaev et al.[41]

TABLE 3: Binding Energies (kcal/mol) for Peroxynitrite−Water Complexes

	dimer			trimer		
	PBE	PBE-TIP4P	PBE-TIP4PFQ	PBE	PBE-TIP4P	PBE-TIP4PFQ
ΔE	−18.5	−15.9	−17.4	−33.6	−30.3	−26.2

TABLE 4: Vibrational Frequencies (cm^{-1}) Obtained as the Maxima in the Computed Vibrational Density of States for Peroxynitrite, Obtained from QM/MM Simulations[a]

	NO1 str	O1NO3 bend	O3O4 str	NO3 str	OONO tors	NO3O4 bend	% error
LDA-TIP4P	1579	1061	875	690	527	386	7.2
BP86-TIP4P	1569	960	823	573	485	363	4.3
PBE-TIP4P	1545	973	834	595	500	374	3.7
PBE-TIP4PFQ	1621	943	803	560	519	341	5.7
PBE (isolated)	1475	983	791	462	445	272	13.4
PBE(harmonic)	1476	1026	841	522	485	297	12.3
exp	1564	931	791	642		375	

[a] Experimental results are taken from refs 16−17. Results for isolated peroxynitrite (normal modes and MD simulation) are shown for comparison.

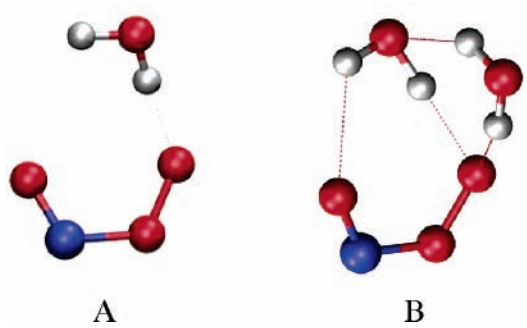

Figure 2. Schematic representation of peroxynitrite−water dimer (A) and trimer (B).

4. QM-MM Molecular Dynamics Simulations

To investigate solvent effects on the peroxynitrite properties, we have performed QM-MM molecular dynamics simulations at the LDA, BP86, and PBE DFT levels, using the mean-field TIP4P potential. In addition, we have also performed simulations of the isolated ion and QM-MM simulations employing the TIP4P-FQ polarizable solvent model at the PBE level. The results obtained from the QM-MM simulation are presented in Table 4. No cis−trans conformational transitions were observed in the MD simulations, consistently with the significant interconversion barrier reported in refs 10 and 17.

As expected, the (anharmonic) vibrational frequencies obtained from the isolated peroxynitrite MD simulation are systematically lower than the harmonic frequencies. The effects of anharmonicity are significant, of the order of 50−60 cm^{-1} in some of the bands.

The vibrational density of states for aqueous peroxynitrite, obtained from the PBE-TIP4P simulation is shown in Figure 3. Each curve corresponds to the Fourier transform of the velocity autocorrelation function of an isolated system normal modes coordinate. Consistently, a large predominance of the original mode is observed in the solution simulation, suggesting that solvation does not change qualitatively the normal modes. In agreement with the experimental Raman results, the band corresponding to the NO3 stretching evidences a very large broadening. This indicates that there are strong solvent effects in the NO3 stretching frequency. The present results, together with the computational results regarding the cis−trans energy difference and interconversion barrier[10,17] rule out the hypothesis of thermal coexistence of the cis and trans conformations in aqueous solution to explain the broadening of this band proposed by Symons.[21]

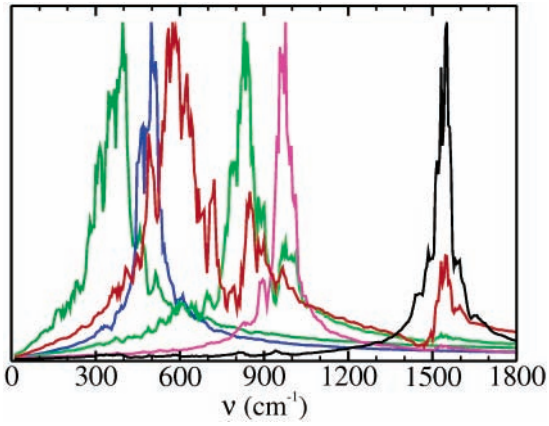

Figure 3. Vibrational density of states computed as the Fourier transform of the velocity autocorrelation function in the isolated species normal modes coordinates for the PBE-TIP4P simulation. (NO1 str, black line; O1NO3 bend, pink line; O3O4 str, green line; NO3 str, red line; OONO tors, blue line; NO3O4 bend, dark green line).

The computed results agree reasonably well with the experiment. The overall errors are small, and the errors in the very sensitive NO3 band are small also, suggesting that our scheme performs reasonably well in describing the system. The results obtained using the more sophisticated TIP4P-FQ model are of similar quality as those obtained using the mean field TIP4P model, implying that even mean-field models are able to capture the most essential features of solvation in this system. The fact that the overall error of the PBE-TIP4P simulation is slightly smaller than that computed at the PBE-TIP4P FQ level may be simply due to error cancellation of the electronic structure scheme and the classical force fields errors.

The interplay of peroxynitrite structure and charge distribution with solvation is analyzed in Figure 4, in which the pair distribution functions, $g_{NO}(r)$, and $g_{OO}(r)$, between the N and O of peroxynitrite with water oxygens, defined as

$$g_{NO}(r) = \left\langle \frac{1}{4\pi r^2}\delta(|r_N - r_{OW}| - r) \right\rangle$$

$$g_{OO}(r) = \left\langle \frac{1}{4\pi r^2}\delta(|r_O - r_{OW}| - r) \right\rangle \quad (3)$$

respectively, are shown for the PBE-TIP4P simulation.

We see a very well defined peak corresponding to O4, confirming that this atom is preferentially solvated because it bears the largest negative charge. Moreover, solvation tends to increase the charge localization on this atom, as can be seen by

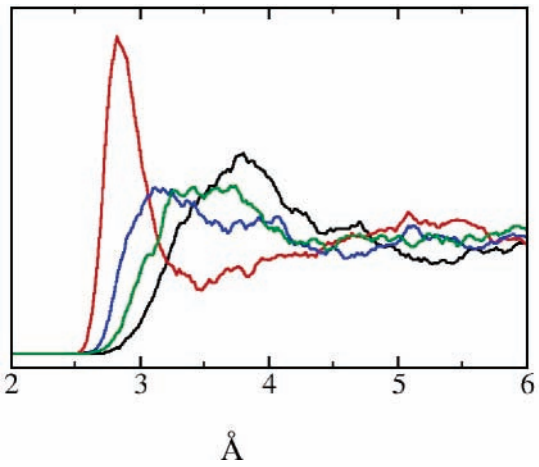

Figure 4. Radial correlation functions for the PBE QM-MM simulation of peroxynitrite atoms with water oxygens. (NOw, black line; O4Ow, red line; O1Ow, green line; O3Ow, blue line).

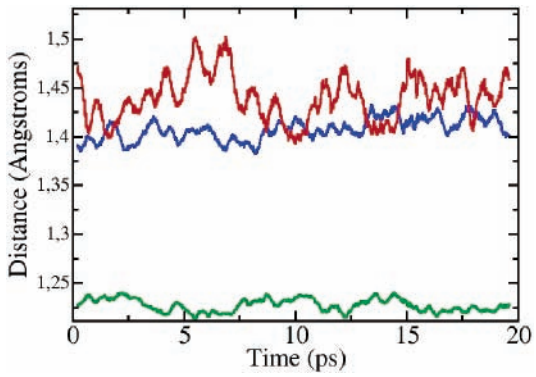

Figure 5. Averaged bond distances (Å) for peroxynitrite as a function of time obtained from the PBE-TIP4P molecular dynamics simulation. (O1N, green line; O3O4, blue line; NO3, red line).

the change in the O4 Mulliken population of the isolated species of −0.598 *e* compared to the mean values of the QM/MM simulation of −0.650 *e* and −0.699 *e* for the TIP4P and the TIP4P-FQ models, respectively. The other two oxygen atoms are less strongly solvated. In addition, as expected, O1 is more efficiently solvated than O2. An estimation of the solvent effects on the vibrational frequencies can be obtained by subtracting the values for the isolated species MD to the result obtained for the QM-MM MD simulation. The estimated solvent shift of 130 cm^{-1} for the NO3 stretching band is significant. It is interesting to notice that continuum solvent models are not able to capture this effect. The fact that the peaks are very broad, reflecting that different solvation patterns are sampled along the simulation, is also consistent with the broad peaks observed in the experimental Raman spectrum, especially for the NO3 stretching band at 642 cm^{-1}.

To obtain further microscopic insight on the interplay between solvation and the unusually broad NO3 stretching band, we have analyzed the time evolution of the vibrationally averaged intramolecular bond distances from the PBE TIP4P molecular dynamics simulation. (Figure 5). It can be observed that the NO3 bond exhibits larger fluctuations than those corresponding to both NO1 and O1O3 bonds. This is consistent with the computed band broadenings in the vibrational DOS. The mean value of the NO3 bond distance of 1.44 Å is smaller than the 1.46 Å obtained for the isolated species optimization, consistently with the fact that the NO3 bond becomes stronger in going from vacuum to solution. Two snapshots, corresponding to peroxynitrite configurations with NO3 bond distances in the extremes of the distribution, namely, 1.50 and 1.40 Å respectively, are depicted in Figure 6. The snapshot with the NO3 bond distance of 1.50 Å exhibits only 2 water molecules coordinating O4. On the other hand, the snapshot corresponding to the NO3 bond distance of 1.40 Å, exhibits a more favorable solvation situation, in which O4 is coordinated with 3 water molecules. This variability in solvation patterns is responsible for the large band broadening observed both in the simulated DOS and in the experimental Raman spectrum.

5. Conclusions

Our QM-MM scheme provides a powerful tool for the investigation of the structural and vibrational spectra of species in solution, because it incorporates in a natural way anharmonicity and solvent effects. In this problematic case, great care should be exercised to employ a QM scheme that yields a reasonable description of the electronic structure of the isolated species. In this case, HF based schemes fail due to a triplet−singlet instability of the HF wave function, but DFT exhibits no instabilities. With the help of the isolated species calculations and QM-MM simulations using both mean-field and polarizable solvent models, a comprehensive microscopic picture of the influence of solvation on the vibrational spectrum of this problem molecule is obtained. Specifically, we have been able

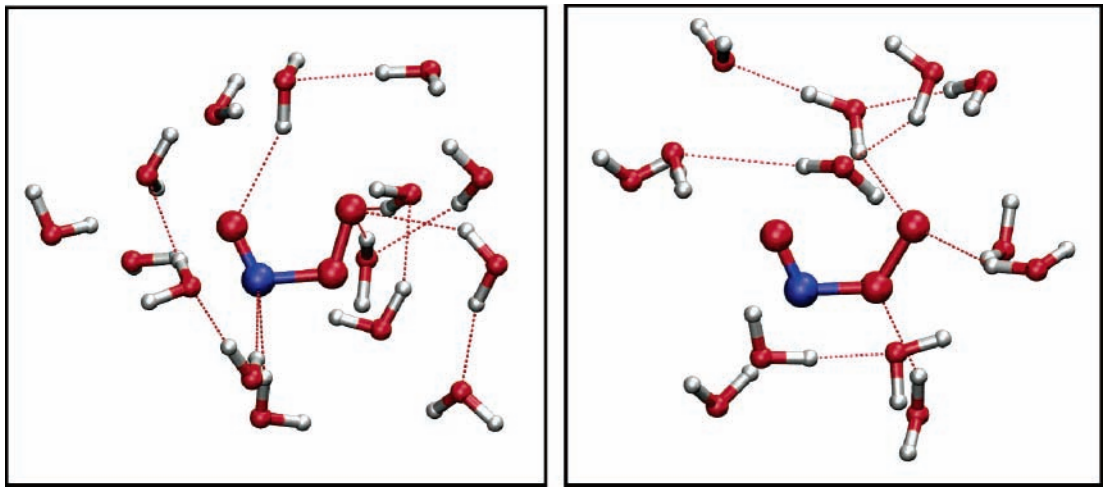

Figure 6. Snaposhots of configurations of aqueous peroxynitrite showing only water molecules in the first solvation shell. Configurations corresponding to NO3 bond distances of 1.40 and 1.50 Å are shown in the left and right panels, respectively.

to shed light on a discrepancy between theory and experiment regarding the broad experimental band at 642 cm^{-1}, which has been assigned to the torsion mode[16,17] but corresponds instead to the NO3 stretching. Solvation not only produces a significant shift of the band but also induces a large broadening, as a consequence of different accessible solvation patterns. Our description allowed us to provide a consistent assignment of the Raman experimental results, reconciling theory and experiment, and to shed light on the interplay between solvation and peroxynitrite properties.

Appendix

MM Cutoff Scheme. A cutoff scheme with a switched electrostatic potential function has been used for dealing with solvent−solvent interactions, according to

$$V(r_{ij}) = q_i q_j (1/r_{ij} + D) \qquad r_{ij} < r_0 \tag{A1}$$

$$V(r_{ij}) = q_i q_j (C - A r_{ij} - B r_{ij}^{\,2}) \qquad r_0 < r_{ij} < r_1 \tag{A2}$$

$$V(r_{ij}) = 0 \qquad r_1 < r_{ij} \tag{A3}$$

The values of the *A*, *B*, *C*, and *D* parameters are obtained by requiring that the potential and its derivative are continuous at the cutoff values. The employed values of r_0 and r_1 were 10 and 12 Å, respectively. A simple cutoff scheme with a value of 12 Å was used for Lennard-Jones interactions.

QM-MM Cutoff Scheme. The electron density of the quantum system is given by

$$\rho(r) = \sum_{i=1}^{N_{\mathrm{Occ}}} |\psi_i|^2 \tag{A4}$$

where each KS molecular orbital, ψ_i is defined as

$$\psi_i = \sum_k c_i^k g_k(r) \tag{A5}$$

Where $g_k(r)$ are the contracted basis functions, given by

$$g_k(r) = \sum_{j=1}^{n} a_k^j f_j(r) \tag{A6}$$

where each $f_j(r)$ is a primitive Gaussian function. Then, the density can be written as

$$\rho = \sum_{i=1}^{N_{\mathrm{Occ}}} |\sum_{k,j} c_i^k a_k^j f_j(r)|^2 \tag{A7}$$

The product of two Gaussians functions of exponents α and β, centered on nuclei A and B respectively, is proportional to another Gaussian function, centered on a point P, according to

$$f_a(\alpha, r-R_A)\, f_b(\beta, r-R_B) = K_{AB} f_c(p, r-R_p) \tag{A8}$$

where the constant K_{AB} is

$$K_{AB} = \left(\frac{2\alpha\beta}{(\alpha+\beta)\pi}\right)^{3/4} \exp\left[-\frac{\alpha\beta}{(a+b)|R_A - R_B|^2}\right] \tag{A9}$$

The exponent of the new Gaussian function centered in R_p is

$$p = \alpha + \beta$$

and R_p is given by

$$R_p = \frac{\alpha R_A + \beta R_B}{\alpha + \beta} \tag{A10}$$

The QM-MM coupling term is given by

$$E_{\mathrm{QM-MM}} = \sum_{l=1}^{N_C} q_l \int \frac{\rho(r)}{|r - R_l|}\, dr + \sum_{l=1}^{N_C} \sum_{\alpha=1}^{N_q} \left[\nu_{LJ}(|R_l - \tau_\alpha|) + \frac{q_l z_\alpha}{|R_l - \tau_\alpha|} \right] \tag{A11}$$

where υ_{LJ} is the Lennard-Jones potential between the classical and quantum part of the system. We can express the first term of eq A11 as

$$\sum_{\alpha=1}^{N_q} q_l \int \frac{\rho(r)}{|r - R_l|}\, dr = \sum_j \sum_{l=1}^{N_C} q_l \int \frac{K_j f_j(p_j, r - R_{p_j})}{|r - R_l|}\, dr \tag{A12}$$

A possible way to compute eq A12 using periodic boundary conditions is to include only the classical point charges located at a distance smaller than R_{cut} from the geometric center of the quantum subsystem. However, this choice turns out to be inadequate in processes in which the spatial extension of the quantum subsystem becomes of the order of R_{cut}. An alternative scheme employed in this work, which alleviates this flaw, consists of using a cutoff scheme in which the integrals for which the classical partial charge is located at a distance larger than R_{cut} from the R_p corresponding to the associated pair of primitive Gaussian functions are neglected. This corresponds to a cutoff scheme in which each Gaussian pair contribution to the total density experiences a cutoff according to its center R_p. The employed R_{cut} value was 12.0 Å.

$$\sum_{l=1}^{N_C} q_l \int \frac{\rho(r)}{|r - R_l|}\, dr \cong \sum_j \sum_{l=1}^{N_C} q_l \int \frac{K_j f_j(p_j, r - R_{p_j})}{|r - R_l|}\, dr \tag{A13}$$

with

$$|R_l - R_{p_j}| < R_{cut}$$

Acknowledgment. This work was partially supported by the University of Buenos Aires, Agencia Nacional de Promoción Científica y Tecnológica (project PICT 06-08447), CONICET (PIP 02508), and Fundación Antorchas. The International Center for Theoretical Physics (ICTP), Trieste, Italy, is acknowledged for hospitality. We thank D. Scherlis for a generous allocation of computer time.

Supporting Information Available: Vibrational density of states for the isolated species at the PBE level, and PBE-TIP4P-FQ, LDA-TIP4P, and BP86-TIP4P QM-MM simulations. This material is available free of charge at http://pubs.acs.org.

References and Notes

(1) (a) Ischiropoulos, H.; Zhu, L.; Beckman, J. *Arch. Biochem. Biophys.* **1992**, *298*, 446−451. (b) Squadrito, G. L.; Pryor, W. A. *Free Radical Biol. Med.* **1998**, *25*, 392−403.

(2) Beckman, J. S.; Ischiropoulos, H.; Zhu, L.; van der Woerd, M.; Smith, C.; Chen, J.; Harrison, J. G.; Martin, J. M.; Tsai, J. H. M. *Arch. Biochem. Biophys.* **1992**, *298*, 438.

(3) Beckman, J. S.; Beckman, T. W.; Chen, J.; Marshall, P. M.; Freeman, B. A. *Proc. Nat. Acad. Sci. U.S.A.* **1990**, *87*, 1620.

(4) Szabo, C. In *Recent Advances in Nitric Oxide Research*; Kitebataka, A., Sakuma, I., Eds.; Springer-Verlag: Tokyo, 1999; pp 1−20.
(5) Wörle, M.; Latal, P.; Kissner, R.; Nesper, R.; Koppenol, W. H. *Chem. Res. Toxicol*. **1999**, *12*, 305.
(6) Cheng, B. M.; Lee, J. W.; Lee, Y. P. *J. Phys. Chem*. **1991**, *95*, 2814.
(7) Merenyi, G.; Lind, J.; Goldstein, S.; Czapski, G. *J. Phys. Chem. A* **1999**, *103*, 5685−5691.
(8) Liang, B.; Andrews, L. *J. Am. Chem. Soc*. **2001**, *123*, 9848−9854.
(9) Koppenol, W. H.; Klasinc, L. *Int. J. Quantum Chem. Biol. Symp*. **1993**, *20*, 1.
(10) Nagy, P. I. *J. Phys. Chem. A* **2002**, *106*, 2659−2670.
(11) Doclo, K.; Rothlisberger, U. *J. Phys. Chem. A* **2000**, *104*, 6464−6469.
(12) Zhao, Y.; Houk, K. N.; Olson, L. P. *J. Phys. Chem. A* **2004**, *108*, 5864−5871.
(13) Houk, K. N.; Condroski, K. R.; Pryor, W. A. *J. Am. Chem. Soc.* **1996**, *118*, 13002−13006.
(14) Tsai, H.; Hamilton, T. P.; Tsai, J. M.; Harrison, J. G.; Beckman, J. S. *J. Phys. Chem*. **1996**, *100*, 6942−6949.
(15) Olson, L. P.; Bartberger, M. D.; Houk, K. N. *J. Am. Chem. Soc*. **2003**, *125*, 3999−4006.
(16) Tsai, J. M.; Harrison, J. G.; Martin, J. C.; Hamilton, T. P.; van der Woerd, M.; Jablonsky, M. J.; Beckman, J. S. *J. Am. Chem. Soc.* **1994**, *116*, 4115−4116.
(17) Tsai, H.; Hamilton, T. P.; Tsai, J. M.; van der Woerd, M.; Harrison, J. G.; Jablonsky, M. J.; Beckman, J. S.; Koppenol, W. H. *J. Phys. Chem*. **1996**, *100*, 15087−15095.
(18) Mak, A. A.; Wong, M. W. *Chem. Phys. Lett.* **2005**, *403* 192.
(19) Harkless, J. A. W.; Rodriguez, J. H.; Mitas, L.; Lester, W. A., Jr. *J. Chem.* Phys. **2003**, *118*, 4987.
(20) Tsai, H. H.; Hamilton, T. P.; Tsai, J. H. M.; Beckman, J. S.; Koppenol, W. H. *Struct. Chem*. **1995**, *6*, 323.
(21) Symons, M. C. R. *J. Inorg. Biochem*. **2000**, *78*, 299.
(22) Warshel, A.; Levitt, M. *J. Mol. Biol*. **1976**, *103*, 227.
(23) (a) Nemukhin, A. V.; Topol, I. A.; Grigorenko, B. L.; Burt, S. K. *J. Phys. Chem. B* **2002**, *106*, 1734−1740. (b) Devi-Kesavan, L. S.; Gao, J. *J. Am. Chem. Soc.* **2003**, *125*, 1532−1540. (c) Diaz, N.; Suarez, D.; Sordo, T. L.; Merz, K. M., Jr *J. Am. Chem. Soc.* **2001**, *123*, 7574−7583.
(24) Nonella, M.; Mathias, G.: Tavan, P. *J. Phys. Chem. A* **2003**, *107*, 8638.
(25) González Lebrero, M. C.; Bikiel, D. E.; Elola, M. D.; Roitberg, A. E.; Estrin, D. A. *J. Chem. Phys.* **2002**, *117*, 2718.
(26) Bikiel, D. E.; di Salvo, F.; González Lebrero, M. C.; Doctorovich, F.; Estrin, D. A. *Inorg. Chem*. **2005**, *44*, 5286.
(27) Kohn, W.; Sham, L. J. *Phys. Rev. A.* **1965**, *140* 1133.
(28) Jorgensen, W. L.: Chandrasekhar, J.: Madura, J. D.: Impey, R. W.; Klein, M. L. *J. Chem. Phys*. **1983**, *79*, 926.
(29) Rick, S. W.; Stuart, S. J.: Berne, B. J. *J. Chem. Phys*. **1994**, *101*, 6141.
(30) Elola, M. D.; Laria, D.; Estrin, D. A. *J. Phys. Chem. A* **1999**, *53*, 5105.
(31) Vosko, S. H.; Wilk, L.; Nusair, M. *Can. J. Phys.*, **1980**, *58*, 1200.
(32) Perdew, J. P. *Phys. Rev. B* **1986** *33*, 8822; **1986** *34*, 7406.
(33) Becke, A. D. *Phys. Rev. A* **1988**, *38*, 3098.
(34) Perdew, J. P.; Burke, K.; Ernzerhof, M. *Phys. Rev. Lett.* **1996** *77*, 3865−3868.
(35) Godbout, N.; Salahub, D. R.; Andzelm, J.; Wimmer, E. *Can. J. Chem*. **1992**, *70*, 560.
(36) Allen, M. P.; Tildesley, D. J. *Computer Simulation of Liquids*; Clarendon: Oxford, U.K., 1987.
(37) Berendsen, H. J. C.; Postma, J. P. M.; van Gunsteren, W. F.; Di Nola, A.; Haak, J. R. *J. Chem. Phys*. **1984**, *81*, 3684−3690.
(38) Ryckaert, J. P.; Ciccotti, G.; Berendsen, H. J. C. *J. Comput. Phys*. **1977**, *23*, 327.
(39) Frisch, M. J.; Trucks, G. W.; Schlegel, H. B.; Scuseria, G. E.; Robb, M. A.; Cheeseman, J. R.; Zakrzewski, J. A.; Montgomery, J. A.; Stratmann, R. E.; Burant, J. C.; Dapprich, S.; Millam, J. M.; Daniels, A. D.; Kudin, K. N.; Strain, M. C.; Farkas, O.; Tomasi, J.; Barone, V.; Cossi, M.; Cammi, R.; Mennucci, B.; Pomelli, C.; Adamo, C.; Clifford, S.; Ochterski, J.; Petersson, G. A.; Ayala, P. Y.; Cui, Q.; Morokuma, K.; Malick, D. K.; Rabuck, A. D.; Raghavachari, K.; Foresman, J. B.; Cioslowki, J.; Ortiz, J. V.; Stefanov, B. B.; Liu, G.; Liashenko, A.; Piskorz, P.; Komaromi, I.; Gomperts, R.; Martin, R. L.; Fox, D. J.; Keith, T.; Al-Laham, M. A.; Peng, C. Y.; Nanayakkara, A.; Gonzalez, C.; Challacombe, M.; Gill, P. M. W.; Johnson, B. G.; Chen, W.; Wong, M. W.; Andres, J. L.; Head-Gordon, M.; Replogle, E. S.; Pople, J. A. *Gaussian 98*, Revision A.1; Gaussian, Inc.: Pittsburgh, PA, 1998.
(40) Becke, A. D. *J. Chem. Phys*. **1993**, *98*, 5648.
(41) Musaev, D. G.; Geletti, Y. V.; Hill, C. L. *J. Phys. Chem. A* **2003** *107*, 5862−5873.